Article

Evolutionary paths of active galactic nuclei and their host galaxies

In the format provided by the authors and unedited

Supplementary Table 1 Image Properties of the Low-z Type 1 AGNs

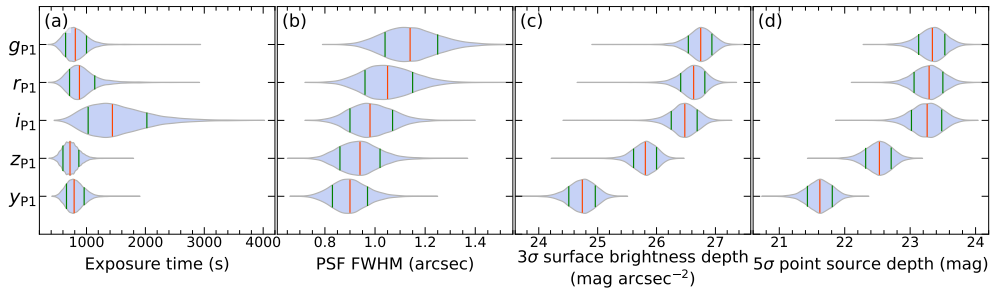| Band	Exposure time	PSF FWHM	3σ surface brightness depth	5σ point source depth
	(s)	(arcsec)	(mag arcsec^{-2})	(mag)
(1)	(2)	(3)	(4)	(5)
g_{P1}	[645, 810, 1000]	[1.04, 1.14, 1.25]	[26.54, 26.75, 26.94]	[23.13, 23.34, 23.53]
r_{P1}	[712, 880, 1140]	[0.96, 1.05, 1.15]	[26.41, 26.63, 26.82]	[23.06, 23.29, 23.50]
i_{P1}	[1028, 1440, 2025]	[0.90, 0.98, 1.07]	[26.25, 26.48, 26.69]	[23.02, 23.26, 23.48]
z_{P1}	[600, 720, 870]	[0.86, 0.94, 1.02]	[25.61, 25.81, 26.00]	[22.32, 22.53, 22.71]
y_{P1}	[660, 790, 960]	[0.83, 0.90, 0.97]	[24.51, 24.74, 24.96]	[21.43, 21.62, 21.81]

Statistics indicate 16th, 50th, and 84th percentiles.

**Supplementary Table 2** Models and Parameters for SED Fitting

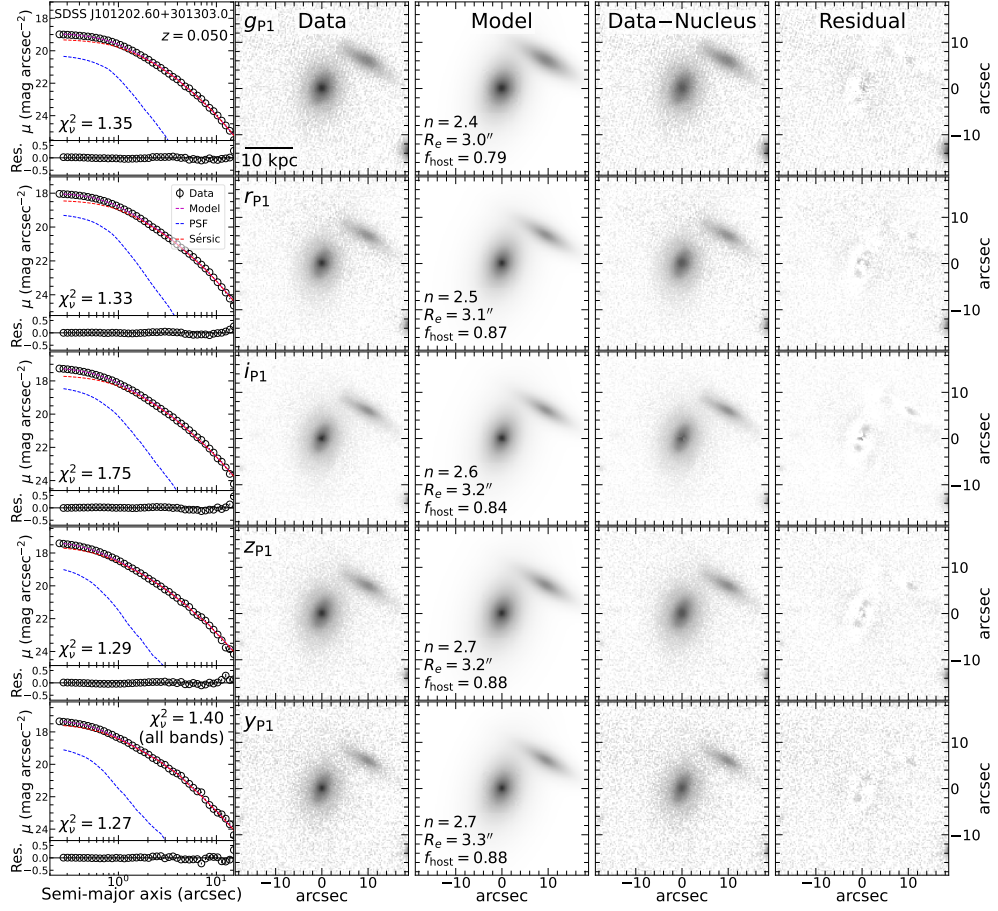| Parameter	Value
Star formation history: delayed	
e-folding time of the main stellar population: τ_{main} (Gyr)	0.001, 0.05, 0.1, 0.25, 0.5, 0.75, 1.0, 1.25, 1.5, 2.0, 2.5, 3.0, 3.5, 4.0, 4.5, 5.0, 6.0, 7.0, 8.0, 9.0, 10, 12, 15, 20
Age of the main stellar population: t_{main} (Gyr)	9.0, 9.5, 10.0, 10.5, 11.0, 11.5, 12.0, 12.5, 13.0
Mass fraction of the latest burst population: f_{burst}	0
Single stellar population: Bruzual & Charlot (2003)	
Initial mass function	Chabrier (2003)
Metallicity	0.02 (solar)
Nebular emission	
Ionization parameter: $\log U$	-2.0
Dust attenuation: modified starburst attenuation law	
The color excess of the nebular lines: $E(B-V)$ (mag)	0.0, 0.001, 0.005, 0.01, 0.03, 0.05 0.1, 0.2, 0.3, 0.4, 0.5, 0.6, 0.8
Ratio of $E(B-V)$ between stellar continuum and emission line	0.44
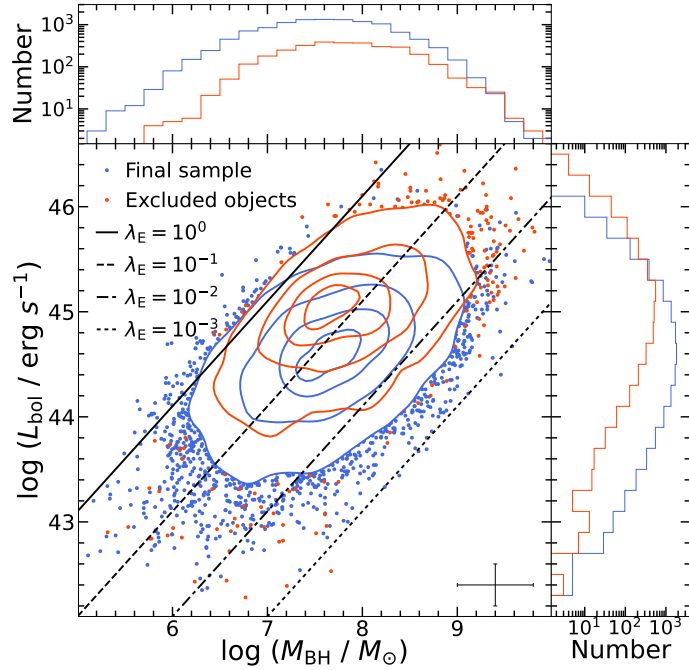
Supplementary Fig. 1 Distribution of AGNs in the final sample (blue) and those that are excluded (red) on the M_{BH} versus L_{bol} plane. Contours indicate the distribution of 10%, 30%, 60%, and 90% of the entire sample, respectively. Dots are individual objects located outside the 90% contour. Solid, dashed, dash-dotted, and dotted lines represent Eddington ratios of $\lambda_{\text{E}} = 10^0, 10^{-1}, 10^{-2}$, and 10^{-3}, respectively. Typical uncertainties in the lower-right corner indicate a conservative 1σ uncertainty of 0.4 dex for M_{BH}.
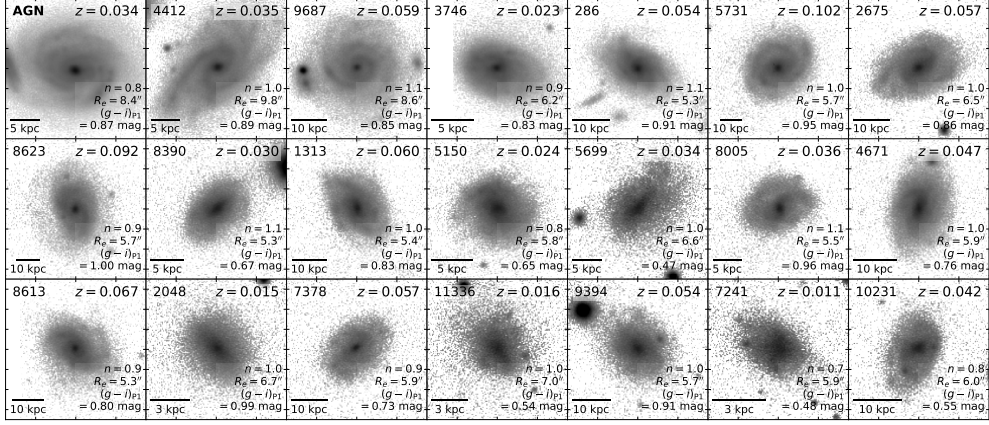

Supplementary Fig. 2 Distributions of image properties of the AGN sample. Panels (a–d) show the distributions of exposure time, PSF FWHM, 3σ surface brightness depth, and 5σ point source depth, respectively. The red and two adjacent green vertical lines indicate the 50th, 16th, and 84th percentiles of the population. σ is the standard deviation of 100 flux measurements made using a circular aperture of diameter $15''$ for extended sources and 2 times the PSF FWHM for point sources, randomly placed in the source-masked background of the image. The statistics are shown in Supplementary Table 1.
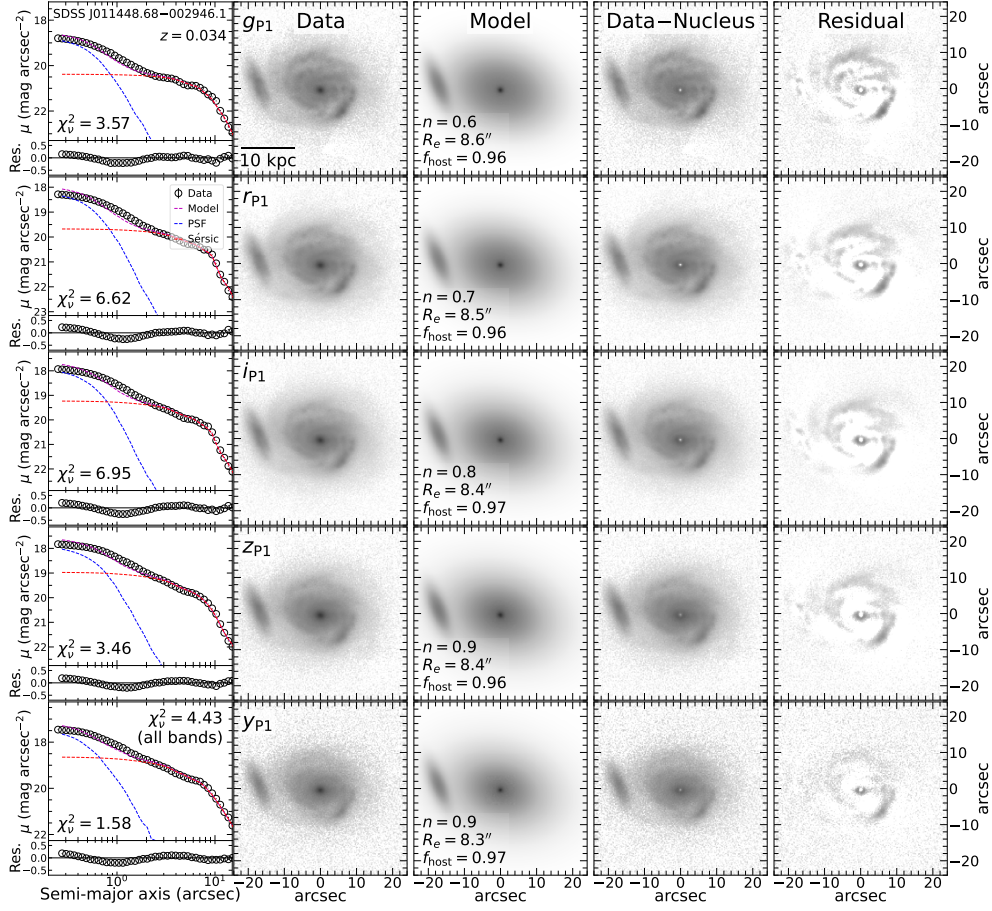
Supplementary Fig. 3 An example of our simultaneous multiwavelength decomposition of SDSS J011448.68−002946.1, a host galaxy with a late-type morphology at $z = 0.034$. Rows from top to bottom are the results for filters $grizy_{\mathrm{P1}}$. The upper panel of the left column shows the radial profile of the surface brightness (open circles with error bars), PSF component (blue), Sérsic component (red), and total (PSF + Sérsic) model (purple). The χ^2_ν from GALFITM for each band is given in the lower-left corner, while that for all five bands is shown in the upper-right corner of the first panel in the bottom row. The lower sub-panel gives the residuals between the data and the model (data−model). The images illustrate, from left to right, the original data, best-fit total model, data with the nucleus component modeled by the PSF subtracted, and residuals of the total model. The best-fit Sérsic index (n), half-light radius (R_e), and host fraction $f_{\mathrm{host}} \equiv$ Sérsic / (PSF + Sérsic) are shown in the third column.

3

Supplementary Fig. 4 An example of our simultaneous multiwavelength decomposition of SDSS J101202.60+301303.0, a host galaxy with a early-type morphology at $z = 0.050$. Rows from top to bottom are the results for filters $grizy_{P1}$. The upper panel of the left column shows the radial profile of the surface brightness (open circles with error bars), PSF component (blue), Sérsic component (red), and total (PSF + Sérsic) model (purple). The χ^2_ν from GALFITM for each band is given in the lower-left corner, while that for all five bands is shown in the upper-right corner of the first panel in the bottom row. The lower sub-panel gives the residuals between the data and the model (data−model). The images illustrate, from left to right, the original data, best-fit total model, data with the nucleus component modeled by the PSF subtracted, and residuals of the total model. The best-fit Sérsic index (n), half-light radius (R_e), and host fraction $f_{\rm host} \equiv$ Sérsic / (PSF + Sérsic) are shown in the third column.

4

Supplementary Fig. 5 An example of a collection of i_{P1} band images of 20 inactive galaxies that have similar structural properties and color as the target AGN (top left panel). The target AGN is the same object in Supplementary Figure 3. Galaxy index and redshift are shown at the top, while the best-fit $(g-i)_{\mathrm{P1}}$ color, half-light radius (R_e), and Sérsic index (n) in the i_{P1} band are shown at the bottom right of each panel.
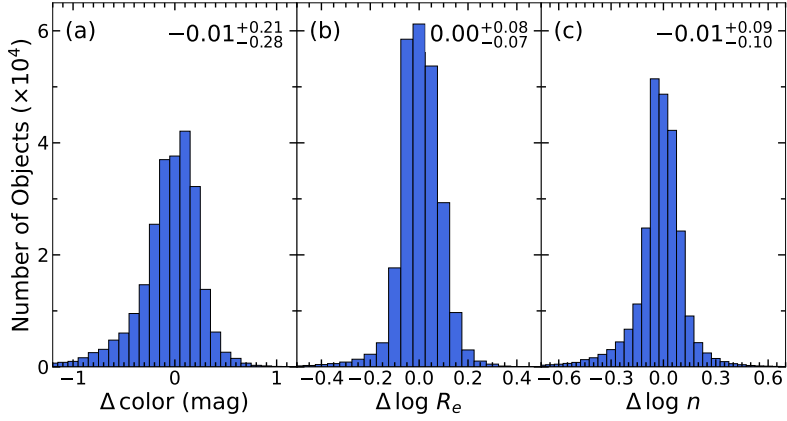

Supplementary Fig. 6 Distributions of the differences ($\Delta = $ AGN−galaxy) between AGNs and inactive galaxies matched in structure and color. Panels (a–c) show the distributions of the differences in observed-frame $(g-i)_{\mathrm{P1}}$ color, R_e, and n in the i_{P1} band, respectively. The median and its differences with 16th and 84th percentiles are shown in the top-right corner of each panel.

5
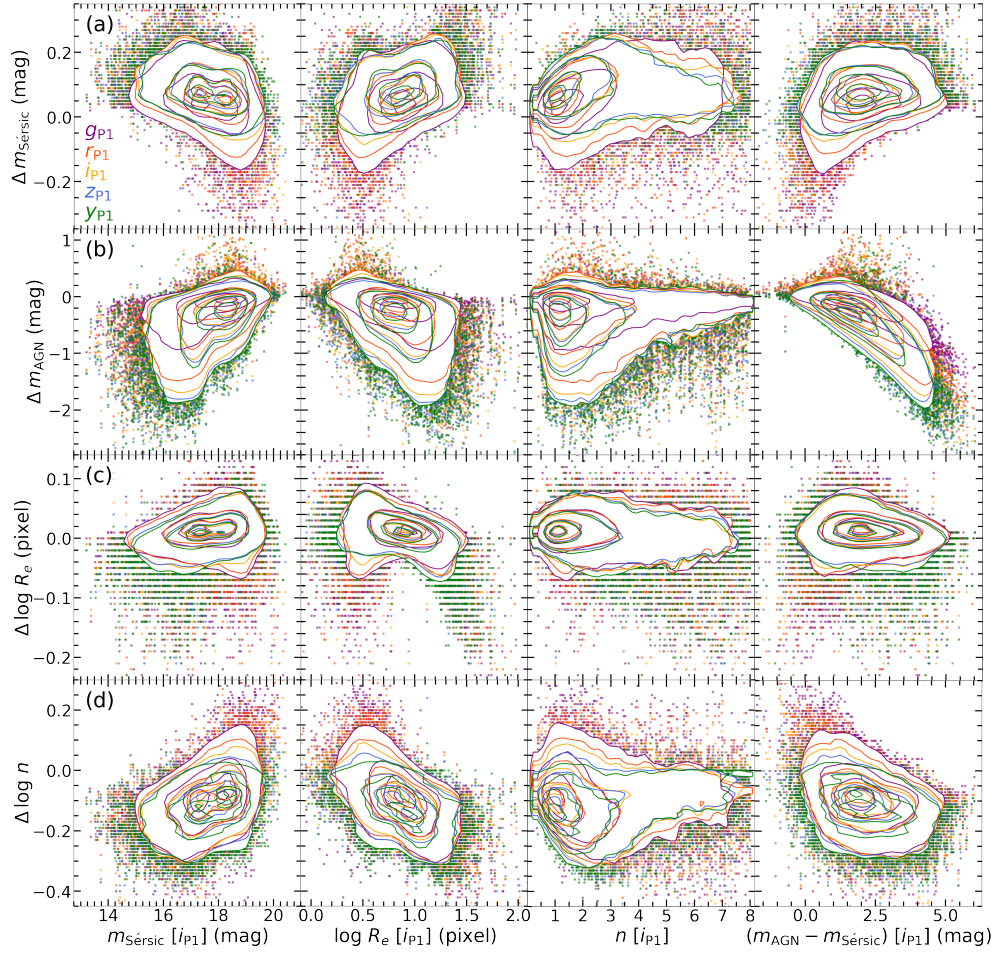
Supplementary Fig. 7 Differences ($\Delta = \mathrm{AGN-galaxy}$) between the results measured in mock AGNs and those measured in the inactive galaxies used to generate the mock AGNs versus AGN properties. Panels (a–d) show differences on $m_{\mathrm{Sérsic}}$, m_{AGN}, R_e, and n versus $m_{\mathrm{Sérsic}}$, R_e, n, and $m_{\mathrm{AGN}}-m_{\mathrm{Sérsic}}$ of the AGN sample, respectively. Purple, red, orange, blue, and green colors represent parameters measured in the $grizy_{\mathrm{P1}}$ bands, respectively. Contours indicate the distribution of 10%, 30%, 60%, and 90% of the entire sample, respectively. Individual dots are the median values of 20 mock AGNs for each AGN target located outside the 90% contour.
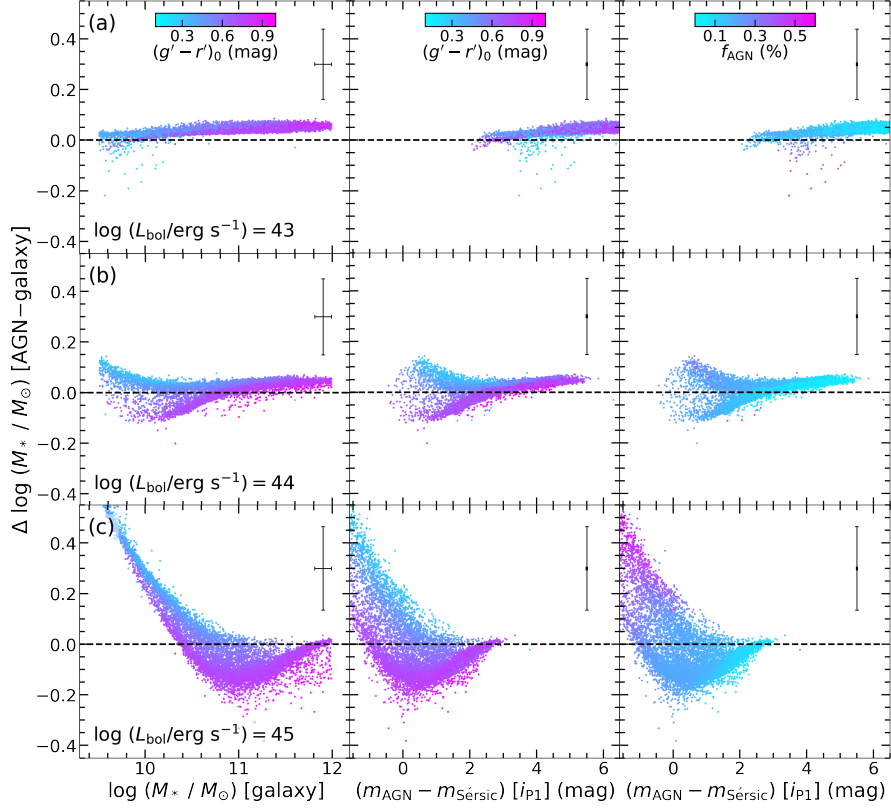
Supplementary Fig. 8 Differences ($\Delta = $ AGN$-$galaxy) between the stellar masses measured in mock AGNs and those measured in the inactive galaxies used to generate the mock AGNs versus AGN properties. Left column shows stellar mass differences versus M_* of inactive galaxies, while middle and right columns show stellar mass differences versus $m_{\mathrm{AGN}} - m_{\mathrm{Sérsic}}$ in the i_{P1} band. Mock are shown for AGNs with (a) $\log(L_{\mathrm{bol}}/\mathrm{erg\ s^{-1}}) = 43$, (b) $\log(L_{\mathrm{bol}}/\mathrm{erg\ s^{-1}}) = 44$, and (c) $\log(L_{\mathrm{bol}}/\mathrm{erg\ s^{-1}}) = 45$. Colors in the left and middle columns represent the rest-frame $(g' - r')_0$ color of the galaxies, and the colors in right column represent f_{AGN} derived from SED-fitting to mock AGNs. Typical uncertainties are shown in the upper-right corner.
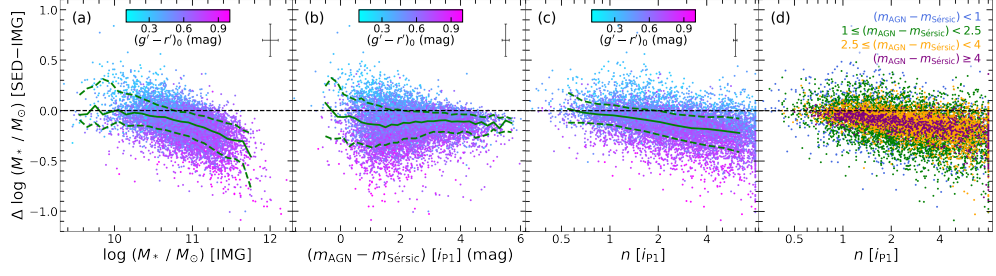
Supplementary Fig. 9 Differences ($\Delta = \mathrm{SED}-\mathrm{IMG}$) between stellar masses of AGNs derived from SED-fitting to AGN+host SEDs (SED) and those from SED-fitting to AGN contribution-subtracted host SEDs from image decomposition (IMG) versus AGN properties. Panel (a) shows stellar mass differences versus M_* from IMG method, panel (b) shows stellar mass differences versus $m_{\mathrm{AGN}}-m_{\mathrm{Sérsic}}$ in the i_{P1} band, while panels (c) and (d) show stellar mass differences versus Sérsic index n in the i_{P1} band. Colors in panels (a), (b), and (c) represent rest-frame optical color $(g'-r')_0$ of galaxies, while colors in panel (d) represent objects with different AGN-to-host contrast ($m_{\mathrm{AGN}}-m_{\mathrm{Sérsic}}$) in the i_{P1} band. Green solid and dashed curves indicate running medians and 16th/84th percentiles of the objects. Typical uncertainties are shown in the upper-right corner.
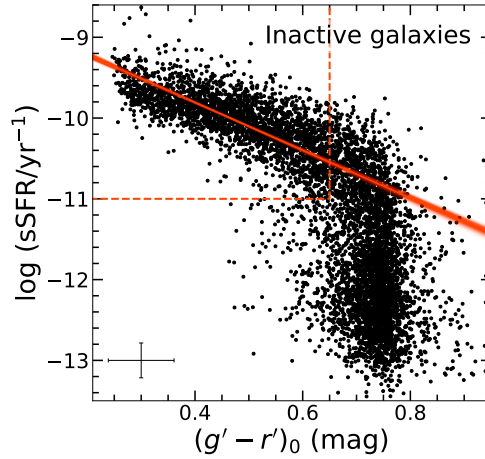
Supplementary Fig. 10 Specific star formation rate (sSFR) versus rest-frame SDSS $g'-r'$ color $[(g'-r')_0]$ for the inactive galaxy sample. The points represent individual objects, with typical errorbars indicating 1σ uncertainty shown in the lower-left corner. The red solid line shows the best-fit linear relation to objects with $(g'-r')_0 < 0.65$ mag and sSFR $> 10^{-11}$ yr^{-1} (above and to the left of the red dashed lines) using `linmix`; the faint lines demarcate uncertainties of the fit.
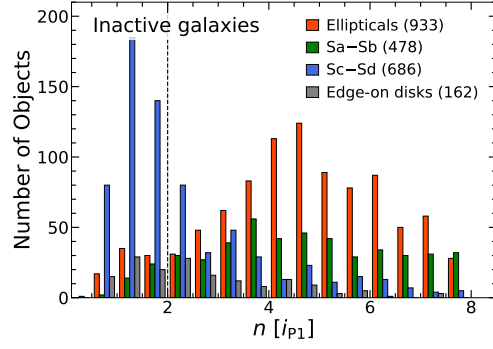
Supplementary Fig. 11 Distribution of Sérsic index n in the i_{P1} band for the inactive galaxy sample. Visual morphological classifications (red: elliptical galaxies; green: Sa−Sb type galaxies; blue: Sc−Sd type galaxies; grey: edge-on disk galaxies) are from the Galaxy Zoo 2 project. The black vertical dashed line at $n = 2$ indicates our criterion to distinguish between late-type, disk-dominated ($n \leq 2$) and early-type, bulge-dominated ($n > 2$) galaxies.
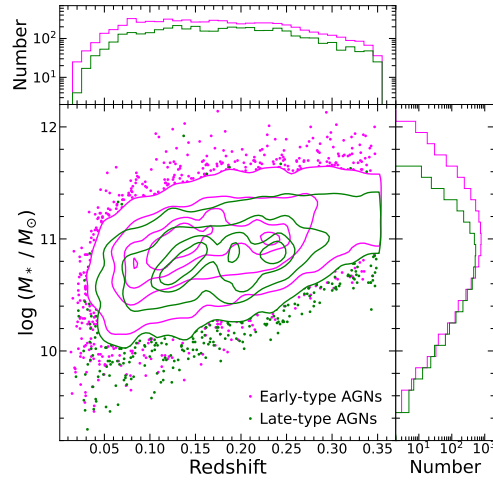
Supplementary Fig. 12 Comparison of redshifts and stellar masses for AGNs with early-type (magenta) and late-type (green) morphologies. Contours indicate the distribution of 10%, 30%, 60%, and 90% of the entire sample, respectively. Dots are individual objects located outside the 90% contour.